**PAPER**

# Impact of cross-sectional geometry on mixing performance of spiral microfluidic channels characterized by swirling strength of Dean-vortices

To cite this article: Lakshmi Balasubramaniam *et al* 2017 *J. Micromech. Microeng.* **27** 095016

View the article online for updates and enhancements.

## Related content

- A planar microfluidic mixer based on logarithmic spirals
Thomas Scherr, Christian Quitadamo, Preston Tesvich et al.

- A novel passive micromixer based on unbalanced splits and collisions of fluid streams
Mubashshir Ahmad Ansari, Kwang-Yong Kim, Khalid Anwar et al.

- Understanding the mixing process in 3D microfluidic nozzle/diffuser systems: simulations and experiments
Abdeljalil Sayah and Martin A M Gijs

# Impact of cross-sectional geometry on mixing performance of spiral microfluidic channels characterized by swirling strength of Dean-vortices

Lakshmi Balasubramaniam⬡, Rerngchai Arayanarakool,
Samuel David Marshall, Bing Li, Poh Seng Lee and Peter C Y Chen[1]

Faculty of Engineering, Department of Mechanical Engineering, National University of Singapore, Singapore

E-mail: mpechenp@nus.edu.sg

## Abstract

Mixing in a microfluidic system is challenging due to dominant diffusion effects at a microscale (low Reynolds number). In this work, we report the improvement of mixing performance in spiral microchannels of varying cross-sectional geometry and hydraulic diameter. The formation of secondary flow interactions in spiral channels, known as Dean vortices, aid the primary diffusion process. The evolution of these Dean vortices was experimentally visualized along the length of the microchannel by confocal microscopy, and then compared to numerical studies. The cross-sectional geometries of the spiral channels, especially in the case of irregular shapes such as the semi-circular and trapezoidal profiles, were found to be an important factor in tuning the strength of Dean vortices, which in turn dictate the mixing performance, as opposed to diffusion which is more prominent at lower Re. This experiment-based finding has been validated via the evaluation of swirling strength of the working fluid, obtained using a numerical study. The results thus obtained show a mixing performance greater than 90% above a Reynolds number of 20 for most spiral channel designs, making this system suitable for high throughput operation with reduced pressure drop. This work is the first to experimentally and numerically demonstrate, within this operating range ($20 < \text{Re} < 277$), the impact on mixing performance in curved microchannels of varying cross-sectional geometries of constant cross-sectional area, and of varying hydraulic diameters for square shaped channels. The capability of these channels to operate at a moderately high Re with enhanced mixing performance and reduced pressure drop would be of great use in large-scale industrial operations, such as complex integrated micro-reactors wherein pressure drop plays a key role.

Keywords: micromixers, Dean vortices, spiral microchannel, microfluidics, laminar flow, microfabrication

Ⓢ Supplementary material for this article is available online

(Some figures may appear in colour only in the online journal)

## 1. Introduction

Miniaturized fluidic systems have become a powerful tool for research in chemistry and physics at a microscale. Small volumes of fluids can be handled and precisely controlled in these systems, thereby enhancing the surface to volume ratio and producing a highly-compact device. In such small devices, however, the important process of fluid mixing becomes challenging due to the mass transport being dominated by slow molecular diffusion. This becomes especially problematic for

---

[1] Author to whom any correspondence should be addressed.

bio-chemical reactions and other analysis procedures requiring controlled and rapid mixing [1–4]. Numerous works suggest methods for improving mass transport in microsystems, via either active or passive approaches. In the active approach, an external force (e.g. acoustic, electrical, pneumatic or magnetic) is applied to create a transversal disturbance, enabling an unstable interface between the two fluids to be mixed [5–8]. Alternatively, in the passive approach, flow energy (e.g. pumping action or hydrostatic potential) is used to create chaotic advection in order to improve mixing performance without the application of an external force. The latter approach is more promising due to the relative ease of system design, fabrication, and integration. In a passive mixer, chaotic advection can be created by geometrical modification such as twisted channels [9, 10], slanted ridges [11, 12], 90° bends [13], zigzagging channels [14–17], embedded barriers [18, 19], curved channels [20–23], and so on. However, most of these geometrically-modified micromixers provide enhanced mixing performance only for low operating flow rates (Re < 100) [12, 15, 20], which might act as a limitation for microreactors which require a larger operating range where diffusion effects are negligible [24]. Additionally, integrated microstructures can dramatically increase pressure drop, resulting in higher total pumping energy for the entire system, especially for those containing complex microfluidic and nanofluidic networks, making the system unusable at higher flow rates. Microstructures and sharp corners within the channels can also create dead zones that lead to fouling formation or air bubbles being trapped inside a microchannel [25]. Furthermore, geometrical modification often requires precise alignment for 3D-structure fabrication, which in turn increases fabrication time and required accuracy [13, 15, 26].

Microfluidic designs with continuous curvature along the channel length, such as spiral channels, can induce secondary flow in the form of Dean vortices, resulting in enhanced mixing [21, 27, 28]. This secondary flow can be generated within a broad operating flow rate suitable for improving mixing time resolution. Moreover, the compact spiral design can yield a system with a small footprint whilst offering greater resistance to fouling formation than that of an equivalent geometrically-modified straight channel—as seen in macro-scale heat exchangers where spiral channels offer a superior fouling resistance [29]. Numerical and experimental demonstrations of curved or spiral channels as micromixers have been reported previously [20–22]. These works have studied the impact of employing spiral (or curved) channel design by adding more layers to the channel system or by employing different methods of curvature to observe how these features affect mixing performance. However, in the vast majority of these studies, either both the hydraulic diameter and the geometry of the cross-section (in a circular or square shape) were kept constant throughout all readings, or the studies were performed purely at a macroscale [28, 30]. In addition, these works characterize flow in a 2D plane through top view imaging, which would be unable to capture the 3D flow profile along the cross-section and allow observation of the process of secondary flow mixing in curved channels. In a numerical study found in the literature involving varying cross-sectional

profiles in a spiral channel, the investigation was conducted in a context not related to mixing in microchannels (namely heat transfer), which would also cause the occurrence of an addition form of mixing (i.e. convection) and, moreover, the results were based entirely on computer simulation without experimental substantiation [31].

In the work reported in this paper, the problem of optimizing the cross-sectional geometry of a spiral channel in order to improve mixing performance is investigated. This study focused on the geometry of the cross-section of the spiral channel, since altering this geometry can lead to improvement in mixing performance (thus reducing mixing time) but does not substantially increase the pressure drop of the entire system. In addition, the hydraulic diameter of a square shaped spiral channel was varied from 300–900 $\mu$m so as to understand the impact of varying hydraulic diameter on mixing performance and pressure drop incurred along the microchannel. Based on the understanding that the formation of the Dean vortices represents an important mechanism that significantly affects the mixing performance of a spiral channel, confocal microscopy was employed to study the evolution of Dean vortices at critical junctions along the entire channel and determine how these geometries affect mixing performance. When this method was applied in experimentally investigating the effect on mixing performance of spiral channels with a set of cross-sectional geometries and hydraulic diameters, it was found that the cross-sectional geometry of the spiral channels, especially in the case of the irregular semi-circular and trapezoidal shapes, was an important factor in tuning the strength of the Dean vortices, observed through an improvement in the mixing performance. This increase in mixing performance was validated via numerical studies, with an improvement in the swirling strength noted for microchannels with an irregularly shaped cross-section.

Although the formation of Dean vortices in microchannels has been reported previously from experimental observations [32] and numerical simulations [26, 33–35], this work is the first to compare the strength of Dean vortices within spiral channels of varying cross-sectional geometry over a broad operating range of flow rates with direct 3D imaging of the dynamical flow patterns in actual microfluidic devices, using numerical studies to support this observation. While comparing the different cross-sectional geometries, the cross-sectional area of the spiral channel was kept constant so that the flow velocity is kept constant throughout.

## 2. Material and methods

### 2.1. Device design and fabrication

This study uses spiral microchannels with a variety of cross-sectional geometry profiles (square, rectangular, semi-circular and trapezoidal) and varying hydraulic diameters (300, 600, 900 $\mu$m) of square-shaped channels, all of which were designed using SolidWorks. The hydraulic diameters ($D_h$) and cross-sectional areas of the different shapes employed in this study are detailed in table 1 and figure S1. The spiral channel was designed to be a logarithmic spiral

**Table 1.** Dimensions of cross-sectional geometries employed.

| Shape | $D_h$ ($\mu$m) | Area ($\mu$m$^2$) |
|---|---|---|
| Square 1 | 300 | 90 000 |
| Square 2 | 600 | 360 000 |
| Square 3 | 900 | 810 000 |
| Semicircle | 585 | 360 000 |
| Trapezoid | 584.2 | 360 000 |
| Tall rectangle | 529.4 | 360 000 |
| Wide rectangle | 529.4 | 360 000 |

with increasing radius of curvature from 1.5–6.5 mm, giving a total length of 77 mm. The channel has two inlets meeting at a *Y*-junction and a single outlet connection at the center. The different geometries were designed so as to keep their cross-sectional area constant, and thus they have varying hydraulic diameter. This allows study of the evolution and strength of Dean vortex strength within different cross-sectional profiles without varying fluid flow velocity. The designs with varied hydraulic diameters have a square-shaped cross-section to solely observe the impact of varying flow velocity on diffusion and Dean vortex formation, which in turn affects mixing performance.

Master molds for the square and rectangular shapes were fabricated in polymer (Prototherm) by stereolithography (Proto Labs Inc., US), while those for the semi-circular and trapezoidal geometries were milled from aluminium (Whits Technologies, Singapore). Different methods of fabrication were employed for these molds to ensure a smooth surface along slopes and curves, thereby minimizing dimensional errors for irregular shapes. Using these master molds as a template, polydimethylsiloxane (PDMS) replicates were fabricated by mixing Sylgard 184 silicone elastomer (Dow Corning, US) with its curing agent in the ratio 10:1 and curing at 60 °C overnight. Upon curing, PDMS was peeled off from the master mold and the inlet and outlet fluidic access holes were punched. The PDMS microchannels were then bonded onto a layer of glass through plasma activation to form a closed channel network. Tygon tubings (Cole-Parmer, US) were then used to facilitate flow passage into these microchannels from a flow control system. During imaging work, the dimensions of the channel were measured to ensure no dimensional changes occur in the channel due to a change in flow velocity.

### 2.2. Numerical modelling

Dean flow and its relative strength for different geometries were simulated using the commercially available CFD software package Ansys FLUENT 15, based on the finite volume method, and meshed using that program's in-built meshing tool. The number of elements used varied from 500 000 to 1 000 000, chosen via a mesh dependency study conducted for each individual geometry. These studies were conducted by solving the Navier–Stokes continuity and convection-diffusion equations by assuming laminar Newtonian flow throughout the microchannel, as well as no-slip boundary

conditions, as described in other works [36–39] and depicted in equations (1)–(3) as:

$$\frac{\partial V}{\partial t} + V \cdot \nabla V = -\frac{1}{\rho}\nabla P + \frac{\mu}{\rho}\nabla^2 V \tag{1}$$

$$\nabla \cdot V = 0 \tag{2}$$

$$\frac{\partial c}{\partial t} + (V \cdot \nabla)\, c = D\nabla^2 c \tag{3}$$

where $V$ is the velocity vector, $\mu$ is the dynamic viscosity, $\rho$ is the fluid density, $P$ is the pressure, $c$ is the concentration of fluids, and $D$ is the diffusion coefficient. The density and viscosity of water were chosen to be 1000 kg m$^{-3}$ and 0.001 Pa s respectively, whilst the diffusion co-efficient was specified to be $2.3 \times 10^{-9}$ m$^2$ s$^{-1}$, based on numerical correlation with experimental results. The solutions were set to be converged if the residual values for continuity and all velocities drop to under $10^{-6}$. The concentrations of stream 1 and 2 at inlet 1 were specified to be 1 and 0 respectively, and at inlet 2 the concentrations of stream 1 and 2 were specified to be 0 and 1 respectively. This numerical model was then validated against existing models [26]. From these simulations swirling strength and mixing performance were obtained at various positions along the spiral length. Swirling strength is defined as the ratio of tangential velocity to core velocity (maximum flow velocity along the streamwise direction) along a given plane [43], and thus acts as an indicator of the vortex strength within the channel [37], permitting assessment of the strength of the Dean vortices formed along the cross sectional plane.

### 2.3. Flow visualization

The utilization of curved channels generates secondary flow in the form of Dean vortices within the fluid. Dean vortices were first studied by Dean as symmetrical vortices generated along the cross-section due to the presence of excess centrifugal force [27]. The presence and strength of these Dean vortices are determined by the Dean number, represented by equation (4) as:

$$\text{De} = \text{Re} * \sqrt{\frac{D_h}{2R}} \tag{4}$$

where $R$ is the radius of curvature. In order to visualize the phenomenon of fluid mixing due to formation of Dean vortices, cross-sectional time-lapse images of two streams of de-ionized (DI) water were obtained using a laser scanning confocal microscope (Olympus) with a 10× objective as illustrated in figure 1. These images were obtained every 90° from the inlet to the outlet, as shown in figure 2. Of the two streams of DI water introduced at the inlet, one stream was tagged with 10 $\mu$M of fluorescein dye (Sigma Aldrich) while the other stream was pure DI water. Flow was introduced into these microchannels using a high-accuracy syringe pump (PHD 2000, Harvard Apparatus) at a constant volume flow rate ranging from 0.1–4000 $\mu$l min$^{-1}$ (highest limit of the pump) through each inlet. The mixing index ($\sigma$) represented
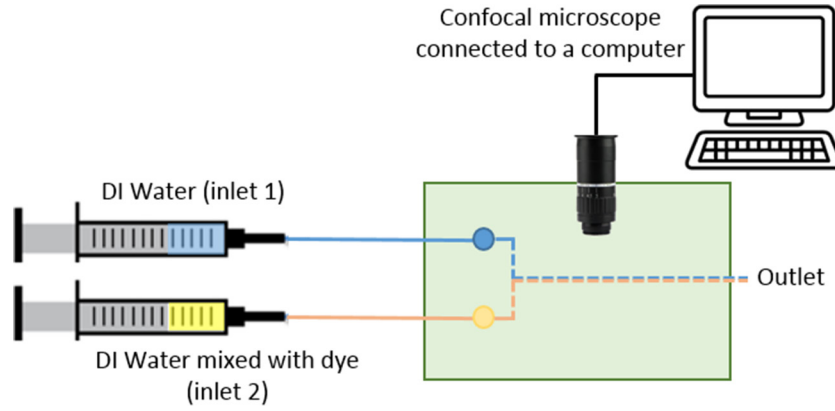
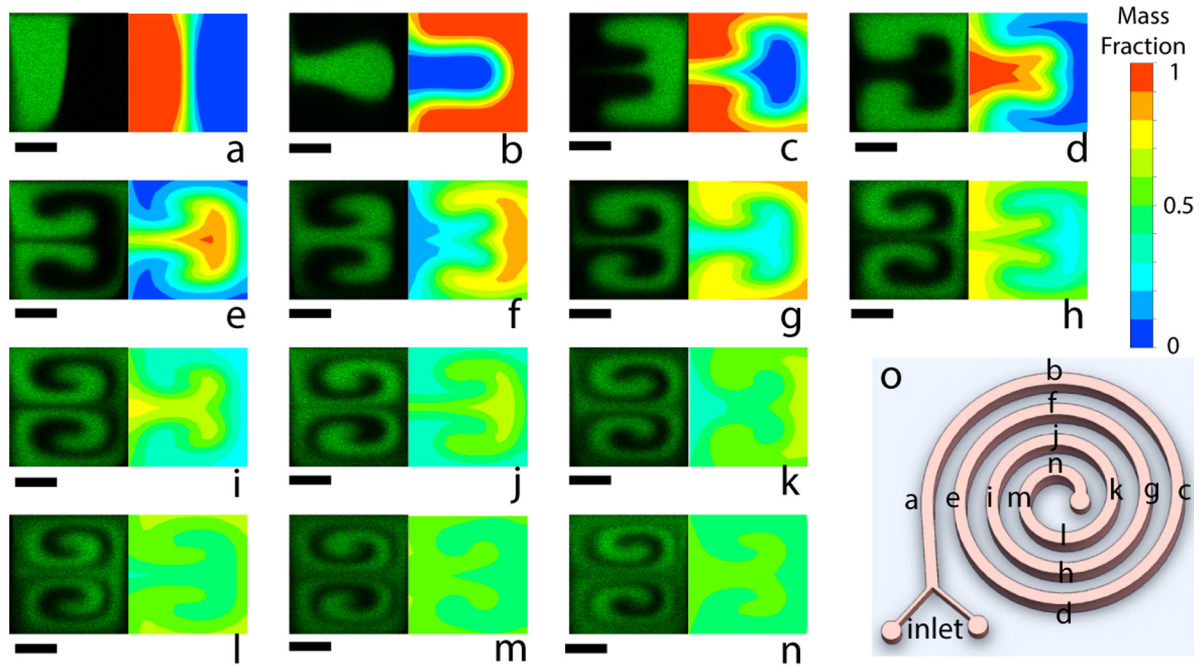**Figure 1.** Illustration of the experimental setup.



**Figure 2.** Illustration of the evolution of Dean vortices in the spiral microchannel from confocal microscope imaging (left) against numerically obtained results of mass fraction (right) along the length of the spiral channel, captured at every 90° bend (a)–(n), as depicted in (o). For confocal microscope imaging, pure water (shown in black) and water solution with fluorescein dyes (shown in green) are introduced at the flow rate of 540 $\mu$l min$^{-1}$ for each stream (Re = 30). The dimensions of the square microchannel are 600 $\mu$m × 600 $\mu$m. Scale bars for all images are 200 $\mu$m.

by the standard deviation of binarized intensity values was then characterized using ImageJ as:

$$\sigma = \sqrt{\frac{1}{n}\sum_{i=1}^{n}\left(I_i - \bar{I}\right)^2} \qquad (5)$$

where $I_i$ is the intensity value at a given point and $\bar{I}$ is the mean intensity value for the given cross-section. A $\sigma$ of 0.5 indicates no mixing while a $\sigma$ of 0 indicates complete mixing. In order to obtain the level of mixing as a performance, the mixing index was modified as: mixing performance $MP = 100 * \left(1 - \frac{\sigma}{\sigma_{max}}\right)$ [17], where $\sigma_{max}$ is the maximum attainable mixing index (0.5). In this way a 100% mixing would indicate complete mixing while 0% would indicate no mixing. Mixing performance was obtained along the cross-section of the channels,

rather than as a top view imaging, so as to capture the effect of Dean vortices within the channel, which gives a more accurate prediction of the level of mixing in these microchannels.

## 3. Results and discussion

### 3.1. Visualization of Dean vortices

Figure 3 illustrates the formation of Dean vortices through the presence of two counter-rotating vortices generated due to an imbalance of the curvature induced centrifugal force and flow velocity in the axial direction. The evolution of secondary flow in the form of Dean vortices is visualized through confocal microscopy (figure 2 *left*) and numerical simulation (figure 2 *right*) along the length of a spiral channel with a square shaped cross-section of hydraulic diameter 600 $\mu$m at
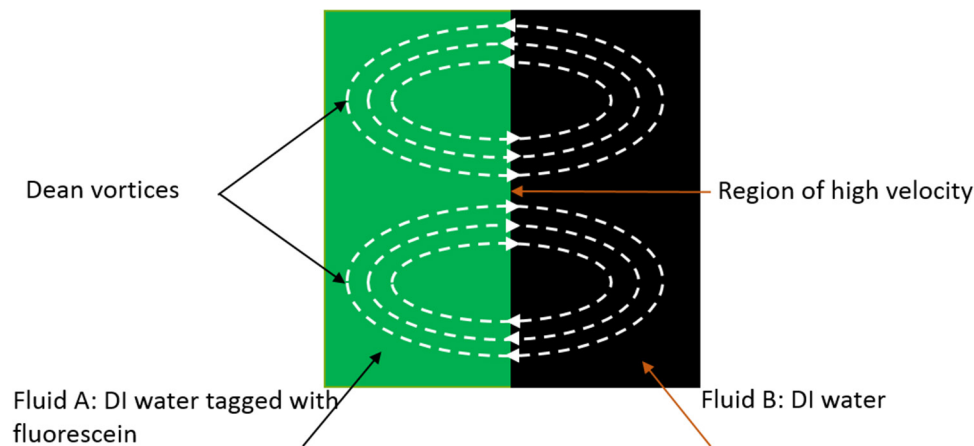
**Figure 3.** Illustration of flow profile and secondary flow formation when Dean vortices occur.

a Reynolds number (Re) of 30. As can be observed in figure 2, although the two fluids enter the channel along the longitudinal direction, secondary flow generated along the channel in the transverse plane pulls one fluid into the other fluid, thereby disrupting the boundary between these two streams as illustrated in figure 3. As the radius of curvature of a spiral channel decreases, these vortices become fully developed and stable, becoming true Dean vortices. The Dean vortices are characterized by the presence of two counter rotating vortices generated on both halves of the plane and are typically observed at Dean number larger than 10 [20] which is reached upon the fluid entering the second loop of the spiral channel design (i.e. figure 2(e) onwards) at the flow velocity shown in figure 2 (Re = 30). In this channel design, flow travels inward from a higher radius of curvature to a lower radius of curvature, thereby strengthening the effect of the Dean vortices due to an increase in Dean number. This provides an insight into how secondary flow evolves into fully developed stable Dean vortices along diverse radii of curvature, thereby enabling the tuning of their strength in order to maximize mixing performance. It also allows an understanding of the impact of varying cross-sectional geometries (square, rectangular, semi-circular and trapezoidal) and hydraulic diameters of spiral microchannels on the strength of Dean vortices and mixing performance.

The formation of Dean vortices in diverse cross-sectional profiles with varying volumetric flow rates are illustrated in figure 4(A), captured just prior to the outlet of the spiral microchannel (in order to avoid exit effects, position shown in figure 2(m)). As observed, in a square channel ($D_\mathrm{h} = 600 \ \mu$m) a low flow rate of 270 $\mu$l min$^{-1}$ (Re = 15) is sufficient to cause initiation of Dean vortices, which then grow stronger, more prominent and more stable as the flow velocity increases. It can also be observed that, prior to the formation of distinctly recognizable Dean vortices (typically observed at Dean number larger than 10 [20]), the fluid profile is still in its nascent state due to an imbalance in the centrifugal forces and pressure forces in the flow. Such a profile can be considered as a precursor to Dean flow. As the radius of curvature decreases or the flow velocity increases, the centrifugal force induced by this change in curvature amplifies the force imbalance, resulting in the formation of distinctively recognizable counter rotating

vortices as observed from figure 2(e). Time lapse images of flow at higher flow velocities also ascertain the stability of these fully developed vortices. An increase in the spread of fluorescence concentration along the cross-section shows that the formation of Dean vortices pulls the two streams into each other, resulting in improved mixing performance. Although the Dean vortices start forming at roughly the same flow rate for all geometries, their strength and effect is more pronounced in trapezoidal and semi-circular microchannels of constant channel area, and in square channels with a smaller hydraulic diameter (especially $D_\mathrm{h} = 300 \ \mu$m).

### 3.2. Improvement in mixing performance

Visualization of Dean vortices generated along the curved channel via confocal microscopy also enables the characterization of mixing performance along the length of this spiral channel, as illustrated in figure 5(A). At a given flow rate, mixing in a spiral channel dramatically increases in comparison to an equivalent straight channel (figure 5(A)) due to the presence of secondary flow along the curved channel which enhances mass transport along the transverse plane. Mixing performance at the outlet for all the cross-sectional geometries with a constant cross-sectional area of 0.36 mm$^2$ are illustrated in figure 5(B) at a flow rate of 540 $\mu$l min$^{-1}$ (Re = 30). Once again, spiral channels are shown to outperform straight equivalents, but from figure 5(B), trapezoid, semi-circular and small square geometries can also be observed to have superior mixing performance in comparison to large square and rectangular cross sectional profiles. Figure 5(C) illustrates a closer look at one of these higher performing geometries (namely the 300 $\mu$m square channel) over a range of flow rates. Dean flow being dependent on flow velocity in turn affects the fluid's Reynolds number (see equation (4)), resulting in a higher mixing performance at higher flow rates for the different cross-sectional geometry designs (figure 6(A)).

From figure 5(C) it can be further verified that as flow velocity increases, mixing between the two flow streams is at first dominated by diffusive forces, followed by a drop in mixing performance at a Reynolds number of 25 and a Péclet (Pe) number of 10 000, before rapidly increasing to a stable value above 90% with a further increase in flow velocity.
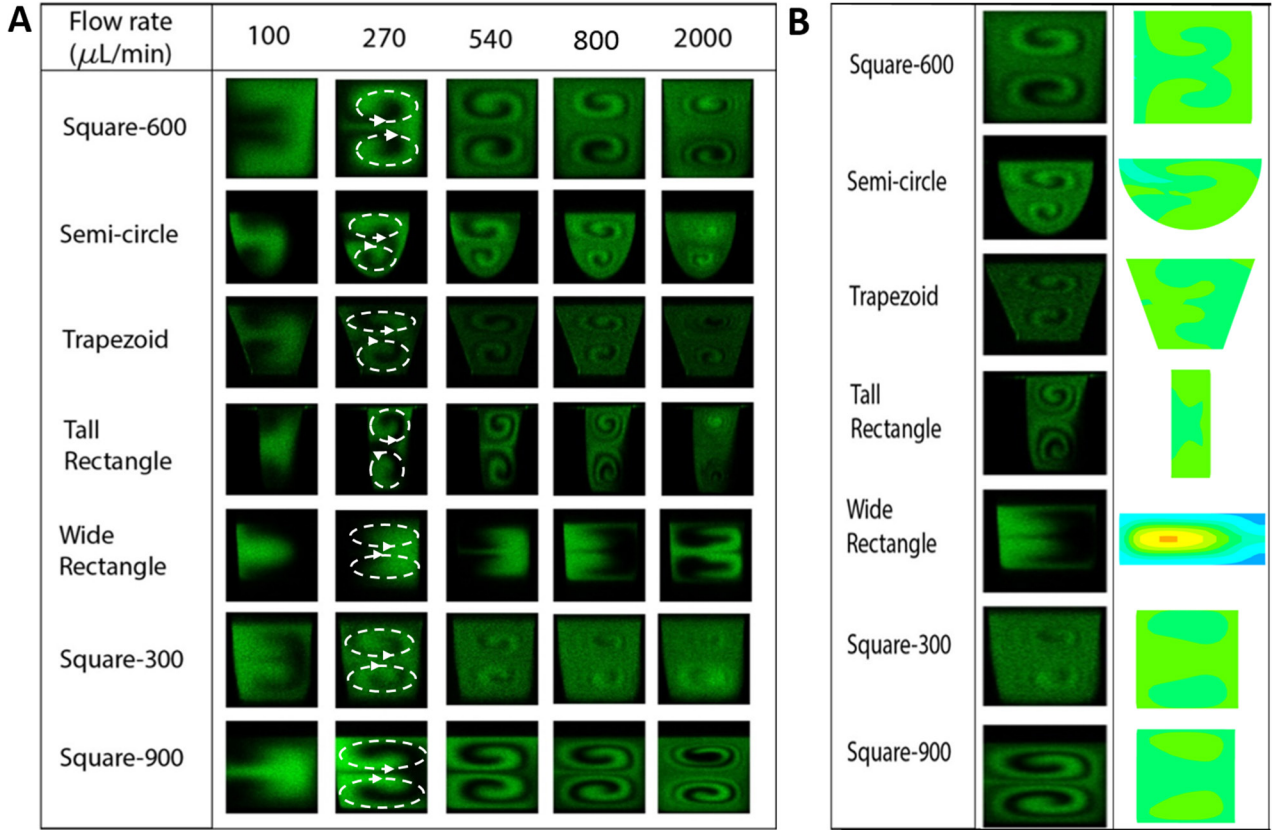
**Figure 4.** Cross-sectional flow profiles just prior to the outlet (position (m) in figure 2) of microchannels with square, tall rectangular, wide rectangular, trapezoidal and semi-circular cross-sections of constant area 0.36 mm$^2$ and with different hydraulic diameters (300, 600, 900 $\mu$m) (A) at different volumetric flow rates (100, 270, 540, 800 and 2000 $\mu$l min$^{-1}$). (B) Comparison of flow profiles at a volumetric flow rate of 800 $\mu$l min$^{-1}$ obtained through confocal imaging and numerical studies. These images were captured using a confocal microscope at a magnification of 10×.
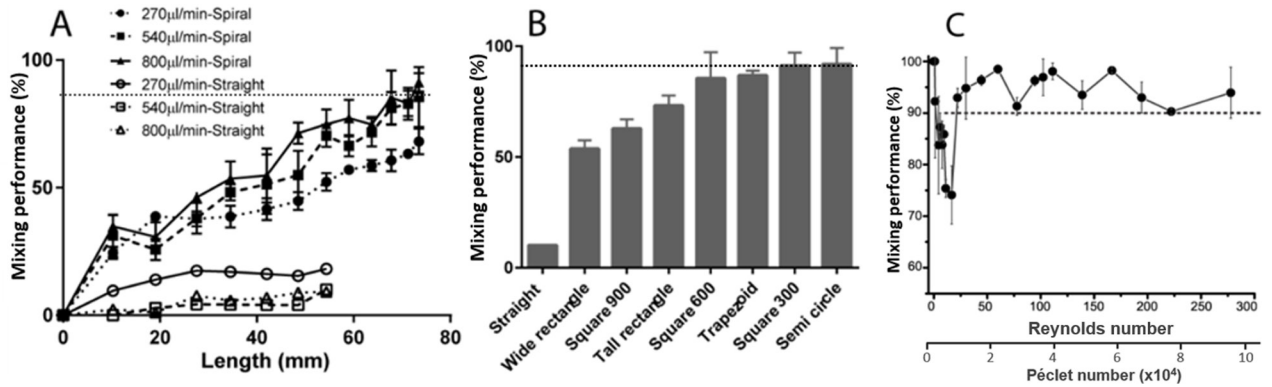


**Figure 5.** (A) Comparison of mixing performance in straight and spiral microchannels of square cross-sectional geometry with dimensions 600 $\mu$m × 600 $\mu$m at three different flow rates (270 $\mu$l min$^{-1}$ or Re = 15, 540 $\mu$l min$^{-1}$ or Re = 30 and 800 $\mu$l min$^{-1}$ or Re = 45). (B) Mixing performance just prior to the outlet of spiral channels with different cross-sectional geometries at a flow rate of 540 $\mu$l min$^{-1}$ (Re ≈ 30 for the geometries with a constant cross sectional area, Re = 60 for a 300 $\mu$m square microchannel and Re = 20 for a 900 $\mu$m square microchannel). (C) The mixing performance just prior to the outlet of 300 $\mu$m × 300 $\mu$m square microchannel over a range of Reynolds numbers.

$$\text{Pe} = \frac{\text{Advective transport rate}}{\text{Diffusive transport rate}} = \frac{D_\text{h} u}{D}. \qquad (6)$$

While at low Re (<1), the mixing inside the 300 $\mu$m square channel is nearly complete since mixing in this flow regime is dominated by molecular diffusion, which is promoted by longer residence time and the resulting interaction of two fluids. When the flow rate increases (1 < Re < 20), two effects are found to occur: the higher convective flow reduces the resident time leading to decreased mixing due to diffusion, and centrifugal forces begin to generate recirculating flow in the transverse plane, enhancing mixing performance via an increase in the resulting Dean number as shown in figure 6(B). At this relatively low Re range, the latter effect
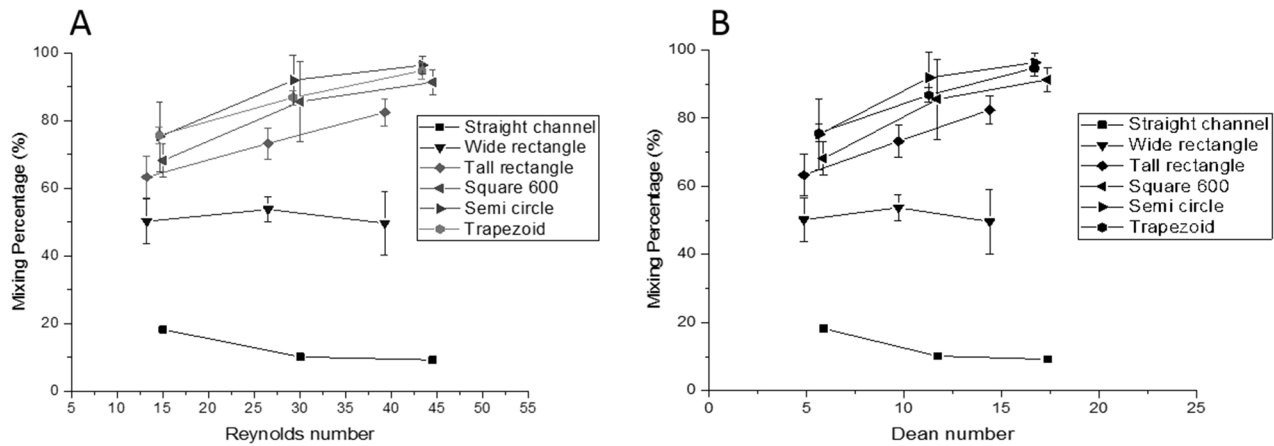
**Figure 6.** Illustration of (A) mixing performance across different Reynolds number (B) mixing performance across different Dean number for a straight square channel and spiral channels with different cross sectional geometry, namely semi-circular, trapezoidal, square, and rectangular.
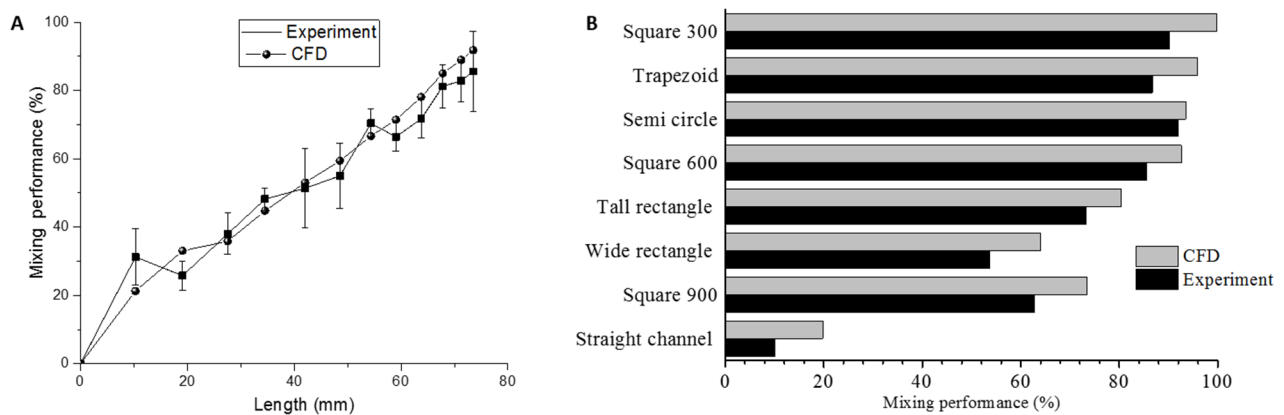


**Figure 7.** Comparison of experimental and numerically obtained mixing performances (A) for a 600 $\mu$m × 600 $\mu$m square microchannel at 540 $\mu$l min$^{-1}$ throughout the length of the channel (B) at the outlet for all geometries at a flow rate of 540 $\mu$l min$^{-1}$.

is not significantly strong enough to perturb axial flow, leading to the noted dip in the mixing performance as the still-dominant diffusion effects weaken. At higher flow rates (Re > 20), the centrifugal force becomes strong enough to trigger secondary flow, leading to higher mixing performance as the slower moving fluid moves from the concave (inner) to convex (outer) walls, as observed in figure S4 (stacks.iop.org/JMM/27/095016/mmedia) where the two velocity cores are pushed towards the outer wall with an increase in flow velocity. It is therefore at this flow rate and above (for this specific channel) that Dean vortices become the dominant effect that determines the amount of mixing within the channel, due to its advective contribution at higher Péclet number.

The mixing performance improvements within square microchannels of varying hydraulic diameter (300, 600 and 900 $\mu$m) at three different volumetric flow rates (270 $\mu$l min$^{-1}$, 540 $\mu$l min$^{-1}$ and 800 $\mu$l min$^{-1}$) are depicted in figure S2. It is shown that a smaller hydraulic diameter generates higher mixing performance (as suggested by figure 5(B)), due to higher flow velocity which results in stronger advective forces in comparison to a channel with a higher hydraulic diameter for a given volumetric flow rate. Additionally, considering a mixing performance of >90% as corresponding to a completely mixed fluid [15], total mixing can be achieved at a flow rate of 540 $\mu$l min$^{-1}$ for a 300 $\mu$m channel and at 800 $\mu$l min$^{-1}$ for a 600 $\mu$m channel. This illustrates that mixing in spiral microchannel is effective at intermediate flow rates (Re > 20) due to the formation of Dean vortices which dominate the weakening diffusion process.

Furthermore, mixing performance was evaluated through a numerical simulation in FLUENT and the results were found to correspond well with those of the experimental studies, as shown in figure 7. For comparison, the flow profiles at location m of figure 2 for the different channels obtained from both experimental and numerical analysis is illustrated in figure 4(B). The mixing performances along the spiral channel for all geometries are shown in figure S2.

Considering the mixing performance at a point just prior to the outlet, at a given constant cross-sectional area, both the experimental and simulation results suggest that the trapezoidal and semi-circular shapes give higher mixing performance as compared to square and rectangular profiles. At a flow rate of 540 $\mu$l min$^{-1}$ (Re = 30) the mixing performance in a semi-circular channel is greater than 90%, whilst in a 600 $\mu$m square channel the same flow rate produces a mixing performance of just 85%, and in the wide rectangular channel a mixing performance of only 54%, as illustrated in figure 7(B).
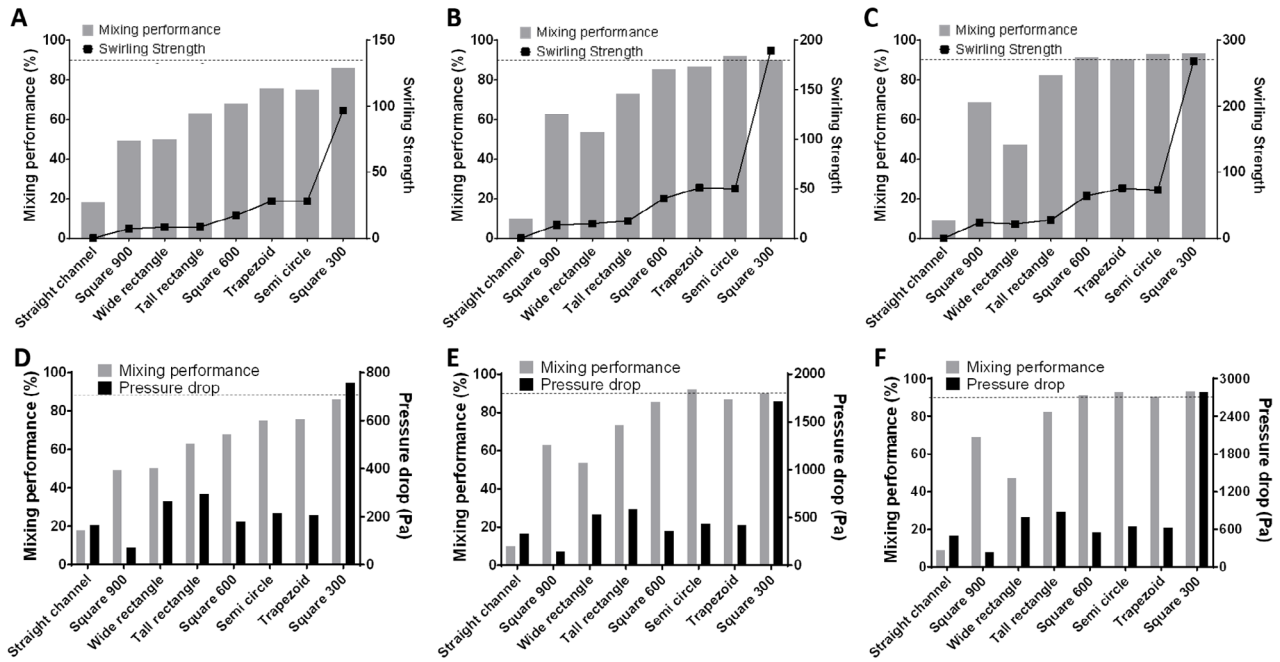
**Figure 8.** (A)–(C) Comparison of numerically obtained swirling strength and experimentally obtained mixing performance to illustrate the relationship between the two parameters at three different flow rates—(A) 270 $\mu$l min$^{-1}$ (B) 540 $\mu$l min$^{-1}$ (C) 800 $\mu$l min$^{-1}$. The dashed line represents a mixing performance of 90%. (D) and (E) comparison of mixing performance and pressure drop for microchannels of different cross-sectional geometries at (D) 270 $\mu$l min$^{-1}$ (E) 540 $\mu$l min$^{-1}$ (F) 800 $\mu$l min$^{-1}$.

To clarify the effect of the semi-circular/trapezoidal geometries on mixing performance, the strength of the vortices formed within a cross-section can be measured by the swirling strength, which is a ratio of the tangential fluid velocity to the core velocity along a given plane. Due to the formation of vortices within the microchannels, the velocity generated at the central core separating the two vortices is very high, resulting in higher swirling strengths in all the curved channels in comparison to the equivalent straight channel, as shown in figure 8. This information can be obtained through CFD simulations for the different geometries (figures 8(A)–(C) and table S2), demonstrating that swirling strength is able to predict the trend observed for mixing performance obtained from the experimental studies. Additionally, the swirling strength of a straight channel is almost negligible at all flow rates (table S2). This can be attributed to the absence of Dean vortices, hence validating the contribution of Dean vortices towards swirling strength. Comparing the swirling strength and mixing performance for the different geometries employed at a fixed area, it can be observed that mixing performance and swirling strength have a positive linear relationship with each other. It is found that the trapezoidal and semi-circular channels achieve the highest mixing performance due to their increased swirling strength via Dean flow along the channel cross-section (figures 8(A)–(C) and table S2) while the mixing performance in a wide channel improves marginally, indicating that the strength of Dean vortices formed is too weak to notably improve mixing within these microchannels. These observations show that changing the cross-sectional geometry of the microchannel allows for control of the strength of Dean vortices within the fluid without impacting the pressure drop, since hydraulic diameter is the key dimension that dictates

the magnitude of pressure drop, as illustrated in figures 8(D)–(F), especially for the 300 $\mu$m channel case. In this way, this method can be utilized instead of the traditional approaches of varying the radius of curvature or flow rate [20, 21, 23] to enhance mixing in microchannels. In this study, since the volumetric flow rate is kept constant, flow velocity within the channel increases by square of the channel size for a reduction in channel size. Since swirling strength grows in magnitude when the flow velocity (proportional to Dean number) within the channel increases, the swirling strength in a smaller channel (300 $\mu$m) is much greater than that in a larger channel (600 $\mu$m). This swirling strength observation corresponds to the results of the present experimental mixing study wherein the mixing performance of a 300 $\mu$m channel is greater than that of a 600 $\mu$m spiral channel.

In the spiral microchannels presented in this study, it can be observed that the formation of secondary flow at $20 < Re < 277$ aids in increasing mixing performance, which is promising and appropriate for applications requiring high operating flow rates, such as industrial micro reactors. It is noted that in the present experiments it was not possible to operate at extremely high flow rates ($Re > 277$) due to the limitations of the visualization instrumentation and fluidic setup. However the device was tested for bonding strength and it can be operated up to $Re = 2400$. The mixing performance in a smaller channel was found to be greater than that in a larger channel, however a 300 $\mu$m channel has a higher pressure drop (more than one order of magnitude) than that of a 600 $\mu$m channel (table S2 and figures 8(D)–(F)). This considerable increase in pressure drop would be a major deterrent in applications where pressure drop would be of great importance, such as an integrated

lab on a chip device consisting of multifunctional units in one single device, microreactors and heat exchanger systems. In addition, the geometry of the cross-section is able to further enhance these Dean vortices by providing more contact surface for rotation of Dean vortices through curvature or slopes, resulting in improved mixing performance in trapezoidal and semi-circular channels. In the case of a wide channel, the vortices generated on both halves spread along the longitudinal direction, causing limited interaction between the top and bottom halves of fluid flow, resulting in a reduced mixing performance. In addition, a wide channel has a smaller depth in comparison to the other channels which reduces the interfacial length of interaction between the two fluids thereby reducing the diffusion component of mixing. Similarly, the non-symmetric nature of irregular shapes such as trapezoid and semi-circular profiles cause the vortices in the two halves to be non-symmetric in shape, forcing vortices in the two halves to interact with each other and match their velocities so as to maintain stability.

On the contrary, several microfluidic mixers reported in the literature can provide high mixing performance only at low Re (<100) [12, 15, 20], limiting their usage for high-throughput system. Moreover, most of these devices contain delicate structures, obstructions and sharp corners along the axial axis which could create an increased pressure drop and additional dead zone areas susceptible to particulate contamination and entrapment of air bubbles. The present spiral channel can instead provide homogenous fluidic flow with reduced dead zone and fouling formation [29]. Furthermore, the presented spiral microfluidic system is fabricated from a single layer of microfluidic chip bonded to a glass substrate, hence reducing fabrication time and potential alignment errors created in 3D structure micromixers due to the several layers and steps in the fabrication process [15, 26]. The high performance and fouling-free system of the presented spiral micromixer design with an irregular cross-section of semi-circle or trapezoid is advantageous for employment in large-scale operations (Re > 20) and within projects requiring low pressure drop penalties such as food, agriculture, and bio-system industries where high-throughput, high-efficiency and highly-controllable micromixers and micro reactors with cost-effective operation (low energy consumption and low maintenance frequency) [25, 40–42] are the basis for design of their microchannel devices.

## 4. Conclusion

In this study it has been demonstrated that mixing performance can be improved through the use of a spiral channel with varying cross-sectional geometry through numerical and experimental correlation. Furthermore a spiral channel produces higher values of swirling strength (and mixing performance) than the minimal swirling strength found in straight channels, making it clear that an additional component of velocity in the tangential direction generated through force imbalance is able to create forced fluidic interactions resulting in improved mixing performance. In addition, the velocity cores generated in the two halves of the channel via the formation of Dean vortices are pushed towards the outer wall, thereby driving the fluid towards the center of the channel in a recirculating fashion. It is also observed that changing the cross-sectional geometry of the spiral channel affects the strength of Dean vortices produced within these channels, as characterized through their swirling strength, suggesting that trapezoid and semi-circular geometry are advantageous. Although the enhancement in mixing performance by changing the cross-sectional geometry is very small, this still provides an understanding as to how cross-sectional geometry influences the early onset of Dean vortex formation, thereby allowing more time for the vortices to stabilize and strengthen as flow moves along the channel of reducing radius of curvature. This strongly suggests that, for spiral channels, mixing performance is not solely a function of the Dean number, but may also vary with cross-sectional geometry. Whilst a 300 $\mu$m channel can achieve higher rate of mixing in comparison to that of a 600 $\mu$m spiral channel of equivalent length and geometry, the pressure drop experienced by flow in a 300 $\mu$m channel is one order higher than that in a 600 $\mu$m channel, which would make operation at higher flow velocities difficult. By contrast, altering the cross-sectional geometry, especially in the cases of trapezoid and semi-circular profiles, which were found to be the most advantageous, can increase mixing performance without significant addition to the microchannel's pressure drop.

Although numerical studies were employed in this study to provide more insight into experimental observation through the measurement of swirling strength, which shows a strong correlation with the experimental observation of mixing performance, this method might not be the optimal way to compare mixing performance in different channels at higher Reynolds numbers (which is a pre-condition for the formation of Dean vortices). This is due to the fact that, at these higher Reynolds numbers (i.e. Re > 45, De > 30), the mixing performances of all channels are found to be close to 100%, making contrast between the different geometries difficult. As such, numerical studies cannot be employed as the sole tool to draw comparison between mixing performance and Dean number, and other visualization based tools should be utilized for verification of results. For these reasons, establishment of an explicit dependence of mixing performance on the Dean number requires deeper analysis that takes the effect of cross-sectional geometry into account. This represents an important direction for future research.

While this study employs a wide range of Reynolds numbers, the principle of varying Dean vortex strength with cross-sectional geometry can be used as an effective strategy to enhance mixing performance, rather than employing flow breakers such as ridges or obstructions, which are both more difficult to manufacture and generate a large pressure drop. In addition, a spiral microchannel as described in this work occupies a smaller footprint area in comparison to that of a straight channel, which would permit easier integration alongside other components in a microreactor. Spiral channels are also known for their fouling resistance making them suitable for use in particle laden applications such as microreactors and heat exchangers.

## Acknowledgment

## Conflict of interest

The authors declare no conflict of interest.

## ORCID iDs

Lakshmi Balasubramaniam   https://orcid.org/0000-0001-6881-8261

## References

[1] Chung B G and Choo J 2010 Microfluidic gradient platforms for controlling cellular behavior *Electrophoresis* **31** 3014–27

[2] Iwasaki T, Kawano N and Yoshida J 2006 Radical polymerization using microflow system: numbering-up of microreactors and continuous operation *Org. Process Res. Dev.* **10** 1126–31

[3] Lu S Y, Watts P, Chin F T, Hong J, Musachio J L, Briard E and Pike V W 2004 Syntheses of C-11- and F-18-labeled carboxylic esters within a hydrodynamically-driven microreactor *Lab Chip* **4** 523–5

[4] Lynn N S, Bockova M, Adam P and Homola J 2015 Biosensor enhancement using grooved micromixers: part II, experimental studies *Anal. Chem.* **87** 5524–30

[5] Jang L S, Chao S H, Holl M R and Meldrum D R 2007 Resonant mode-hopping micromixing *Sensors Actuators* A **138** 179–86

[6] Zahn J D and Reddy V 2006 Two phase micromixing and analysis using electrohydrodynamic instabilities *Microfluid. Nanofluid.* **2** 399–415

[7] Cola B A, Schaffer D K, Fisher T S and Stremler M A 2006 A pulsed source-sink fluid mixing device *J. Microelectromech. Syst.* **15** 259–66

[8] Qian S and Bau H H 2005 Magneto-hydrodynamic stirrer for stationary and moving fluids *Sensors Actuators* B **106** 859–70

[9] Li J, Xia G and Li Y 2013 Numerical and experimental analyses of planar asymmetric split-and-recombine micromixer with dislocation sub-channels *J. Chem. Technol. Biotechnol.* **88** 1757–65

[10] Xia G, Li J, Tian X and Zhou M 2012 Analysis of flow and mixing characteristics of planar asymmetric split-and-recombine (P-SAR) micromixers with fan-shaped cavities *Ind. Eng. Chem. Res.* **51** 7816–27

[11] Stroock A D, Dertinger S K W, Ajdari A, Mezic I, Stone H A and Whitesides G M 2002 Chaotic mixer for microchannels *Science* **295** 647–51

[12] Johnson T J, Ross D and Locascio L E 2002 Rapid microfluidic mixing *Anal. Chem.* **74** 45–51

[13] Yi M Q and Bau H H 2003 The kinematics of bend-induced mixing in micro-conduits *Int. J. Heat Fluid Flow* **24** 645–56

[14] Lee C Y, Lin C F, Hung M F, Ma R H, Tsai C H, Lin C H and Fu L M 2006 Experimental and numerical investigation into mixing efficiency of micromixers with different geometric barriers *Mater. Sci. Forum* **505–7** 391–6

[15] Yasui T *et al* 2011 Microfluidic baker's transformation device for three-dimensional rapid mixing *Lab Chip* **11** 3356–60

[16] Mengeaud V, Josserand J and Girault H H 2002 Mixing processes in a zigzag microchannel: finite element simulations and optical study *Anal. Chem.* **74** 4279–86

[17] Hossain S, Ansari M A and Kim K-Y 2009 Evaluation of the mixing performance of three passive micromixers *Chem. Eng. J.* **150** 492–501

[18] Singh M K, Anderson P D and Meijer H E H 2009 Understanding and optimizing the SMX static mixer *Macromol. Rapid Commun.* **30** 362–76

[19] Tsai R-T and Wu C-Y 2011 An efficient micromixer based on multidirectional vortices due to baffles and channel curvature *Biomicrofluidics* **5** 014103

[20] Sudarsan A P and Ugaz V M 2006 Multivortex micromixing *Proc. Natl Acad. Sci. USA* **103** 7228–33

[21] Sudarsan A P and Ugaz V M 2006 Fluid mixing in planar spiral microchannels *Lab Chip* **6** 74–82

[22] Wang J, Zhan Y, Ugaz V M and Lu C 2010 Vortex-assisted DNA delivery *Lab Chip* **10** 2057–61

[23] Verma M K S, Ganneboyina S R, Vinayak R R and Ghatak A 2008 Three-dimensional multihelical microfluidic mixers for rapid mixing of liquids *Langmuir* **24** 2248–51

[24] Mitic S, van Nieuwkasteele A W, van den Berg A and de Vries S 2015 Design of turbulent tangential micro-mixers that mix liquids on the nanosecond time scale *Anal. Biochem.* **469** 19–26

[25] Schoenitz M, Grundemann L, Augustin W and Scholl S 2015 Fouling in microstructured devices: a review *Chem. Commun.* **51** 8213–28

[26] Yang J, Qi L, Chen Y and Ma H M 2013 Design and fabrication of a three dimensional spiral micromixer *Chin. J. Chem.* **31** 209–14

[27] Dean W R 1928 The stream-line motion of fluid in a curved pipe (second paper.) *Phil. Mag.* **5** 673–95

[28] Howell P B Jr, Mott D R, Golden J P and Ligler F S 2004 Design and evaluation of a Dean vortex-based micromixer *Lab Chip* **4** 663–9

[29] Genic S B, Jacimovic B M, Jaric M S and Budimir N J 2013 Analysis of fouling factor in district heating heat exchangers with parallel helical tube coils *Int. J. Heat Mass Transfer* **57** 9–15

[30] Ligrani P M and Niver R D 1988 Flow visualization of Dean vortices in a curved channel with 40 to 1 aspect ratio *Phys. Fluids* **31** 3605

[31] Kurnia J, Sasmito A and Mujumdar A 2012 Laminar convective heat transfer for in-plane spiral coils of noncircular cross sections ducts: a computational fluid dynamics study *Therm. Sci.* **16** 109–18

[32] Nivedita N, Ligrani P and Papautsky I 2013 Evolution of secondary Dean vortices in spiral microchannels for cell separations *17th Int. Conf. on Miniaturized Systems for Chemistry and Life Science (Freiburg, Germany)*

[33] Schonfeld F and Hardt S 2004 Simulation of helical flows in microchannels *AIChE J.* **50** 771–8

[34] Fodor P S, Vyhnalek B and Kaufman M 2013 Entropic evaluation of Dean flow micromixers *Proc. of 2013 COMSOL Conf. (Boston)*

[35] Al-Halhouli A A, Alshare A, Mohsen M, Matar M, Dietzel A and Büttgenbach S 2015 Passive micromixers with interlocking semi-circle and omega-shaped modules: experiments and simulations *Micromachines* **6** 953–68

[36] Sidharthan S, Gandhi A D, Balashanmugam N and Jeyaraj P 2014 Numerical approach for fabrication of micromixers using microstereolithography *Proc. Mater. Sci.* **5** 527–34

[37] Hussong J, Lindken R, Pourquie M and Westerweel J 2009 *IUTAM Symp. on Advances in Micro- and Nanofluidics* ed M Ellero *et al* (Netherlands: Springer) pp 191–205

[38] Kumar V, Aggarwal M and Nigam K D P 2006 Mixing in curved tubes *Chem. Eng. Sci.* **61** 5742–53

[39] Rudyak V and Minakov A 2014 Modeling and optimization of Y-type micromixers *Micromachines* **5** 886–912

[40] Neethirajan S, Kobayashi I, Nakajima M, Wu D, Nandagopal S and Lin F 2011 Microfluidics for food, agriculture and biosystems industries *Lab Chip* **11** 1574–86

[41] Hartman R L 2012 Managing solids in microreactors for the upstream continuous processing of fine chemicals *Org. Process Res. Dev.* **16** 870–87

[42] Kockmann N, Engler M and Woias P 2005 Particulate fouling in micro-structured devices *Proc. of 6th Int. Conf. on Heat Exchanger Fouling and Cleaning-Challenges and Opportunities Engineering Conf. Int. (Kloster Irsee, Germany, 5–10 June 2005)* ed H Müller-Steinhagen *et al*

[43] Ansys 2017 10.1.8. Vortex Core Region (online) Available at: www.sharcnet.ca/Software/Ansys/16.2.3/en-us/help/cfd_post/vort-core_details_v.html (Accessed: 2 July 2017)